Iranian Polymer Journal (2019) 28:611–620
https://doi.org/10.1007/s13726-019-00728-0

ORIGINAL RESEARCH

Polypropylene–clay micro/nanocomposites as fused deposition modeling filament: effect of polypropylene-*g*-maleic anhydride and organo-nanoclay as chemical and physical compatibilizers

Masoud Salavati[1] · **Ali Akbar Yousefi**[2]

Received: 2 March 2019 / Accepted: 17 June 2019 / Published online: 22 June 2019

Abstract
Amongst various polymers used as fused deposition modeling filaments, polypropylene is one which undergoes rigorous shrinkage during printing. This is a drawback for 3D-printer process and related applications, and to overcome this hurdle, mostly, mineral fillers are utilized; however, this additive reduces mechanical properties. To enhance mechanical and shrinkage properties, unmodified clay sheets extracted from bentonite mineral were used as a reinforcing agent, polypropylene grafted maleic anhydride (PP-*g*-MA) and nanoclay were used as compatibilizers. The compounding was carried out by a twin-screw extruder rather than a single-screw extruder to procure filaments. Afterwards, with fused deposition modeling, dumb-bells and disks were produced for testing. Scanning electron microscopy was employed to examine the morphological feature and dispersion of nanoclay and montmorillonite in the composites. X-ray diffraction was also used to study the dispersion of the nanoclays. The composite disks and dumb-bells were fabricated with a 3D printer to evaluate their rheological properties. Our results showed that the complex viscosity decreased drastically due to aligning the polymer chains along the clay sheets. Mechanical property measurements revealed that the tensile modulus was improved by 60% compared to that of the PP.

Keywords Polypropylene · Fused deposition modeling · Nanoclay · Nanocomposite · Rheology · Mechanical properties

Introduction

Polypropylene is a material utilized in many general purpose products, due to its high mechanical properties, good processability, and low cost [1]. There is a constant urge for optimization of polymers and their additives, therefore, using nanoparticles to improve different properties of the polymers as well as new production methods such as 3D-printing is required [2, 3]. Nanoclay was first employed in nylon-6/montmorillonite (Mt) composite in Toyota Research Center, which made a significant improvement in the mechanical and thermal properties of organic materials with a low solid content [4, 5]. Afterwards, many other research works have been conducted to examine nanoclay effects on nanocomposites with different polymers, modifiers, and processing conditions [6].

PP with different molecular weights has been used as composite with nanoclay and PP-*g*-MA as a compatibilizer to determine the compatibilizer effect on de-lamination. Results showed that in higher molecular weight polymers dispersion is much better because of better shear transfer from screw to nanoclay agglomerates. As polymer molecular weight is decreased, the mixing temperature should be decreased to compromise the missing shear [7]. The higher contents of Mt would result in higher chain scission which can be interpreted relatively to good or poor intercalation acclaimed in processing sequence due to higher shear viscous degradation [8]. Various PP-*g*-MA contents were prepared to determine dispersion behavior of nanoclay in PP matrix. It was found that the optimum PP-*g*-MA amount for compatibilization is within 10–25 wt% range. It was concluded that addition of PP-*g*-MA improves shear transfer to nanoclay sheets which leads to better intercalation, lower mixing temperature, and finally shorter mixing time

✉ Ali Akbar Yousefi
a.yousefi@ippi.ac.ir

[1] Amirkabir University of Technology, Mahshahr Campus, Bandar Mahshahr, Khuzestan, Iran

[2] Department of Plastics, Iran Polymer and Petrochemical Institute, Tehran, Iran

[9]. Different types of PP-*g*-MA were employed at different contents of OMT to study the changes in the intercalation of nanoclay layers of nanocomposites. It was inferred that PP-*g*-MA can enhance the mechanical properties of nanocomposite, though the increase in PP-*g*-MA content, beyond optimum concentration hindered diffusion of polymer chains between the clay galleries [10]. PP-*g*-MA was used with 1 and 4 wt% grafted maleic anhydride content to study its effect on clay dispersion in PP matrix. Their study showed that even though the dispersion was improved in the presence of compatibilizers, some nanoclay layers remained untouched or semi-intercalated due to poor interactions between the polymer and nanoclay or because the layers could not overcome the energy barrier required for nanoclay exfoliation [11].

Chemically modified orgono-modified montmorillonite (OMT) with trimethoxy-(octadecyl)silane (OTMS) was used for further improvement in exfoliation of clay sheets in addition to using PP-*g*-MA. They found higher intercalation values were obtained with the use of PP-*g*-MA and OTMS, and thus, the mechanical and rheological properties were increased [12]. Afterwards, there were some studies to make hybrid micro/nanocomposites to simultaneously improve the dispersion of both micro and nanoparticles. Chen et al. incorporated nano-calcium carbonate ($CaCO_3$) along with nanoclay in a polypropylene matrix and observed that intercalation of nanoclay and mechanical properties were boosted [13]. Micro-$CaCO_3$ particles were employed in combination with nanoclay in PP matrix and surprisingly, the measured mechanical properties in micro/nanocomposite and the rheological properties were higher in case of micro/nanocomposite compared to those micro-composites containing the same amount reported in literature [14].

Nano-sized and micro-sized $CaCO_3$ were combined in PP matrix and stated that this combination highly improved the mechanical properties. A synergistic impact behavior was observed for such a hybrid composite so that the impact strength of the hybrid composite was clearly higher than that of parent non-hybrid composites [15]. This is the closest finding in our approach in spite of the type of reinforcement.

PP linear fiber arrays were used to construct scaffolds by adding layers of PP in electrospinning. This additive manufacturing provided that PP and other polymers with high crystallinity can be used in this method [16]. PP was reinforced with hemp, gypsum, and harakeke and turned into filaments; and those filaments were used in 3D-printer to produce dumb-bells. They observed high contents of additive would result in dimensional instability, but the tensile strength and Young's modulus were improved. The best fiber to reduce shrinkage was harakeke fiber which resulted in a significant lower shrinkage [17]. In another research, filaments of polypropylene-short glass fiber composites were used in fused deposition modeling (FDM) process and good printing quality was reported. They compared the rheology of compression molding with 3D-printing method and that storage modulus increased by adding fibers in compression molding, but surprisingly in 3D-printing, by adding glass fibers, the storage modulus decreased [18].

This work reports on the use of organically modified nanoclay as a compatibilizer between polypropylene and non-modified (natural) microclay composite. The resulting hybrid nano/microcomposite was used as a fusion deposition modeling (FDM) filament to study the rheological and mechanical properties. The novelty of this research lies in using organically modified nanoclay as a dispersion promoter of non-modified microclay.

Experimental

Materials

PP was supplied by Maroon Petrochemical Company (Mahshahr, Iran) (Moplen Z30S grade, MFI = 25 g/10 min and density = 0.9 g/cm^3). The PP-*g*-MA was purchased from Rayan Baspar (Tehran, Iran) (RP79MAC grade, MFI = 20 g/10 min and density = 0.91 g/cm^3). The organo-modified montmorillonite (Cloisite 20A grade) was procured from Southern Clay (presently BYK, USA). Raw bentonite (Bent) was purchased from Zamin Kav Mining Company (South Khorasan, Iran).

Methods and characterization

The clay was extracted by inducing shear in Bent soil in an aqueous medium using a mechanical mixer. After Mt layers were swollen within a day, most small or non-layered silicate minerals could not absorb water. Therefore, the resulting slurry was filtered on a 500-mesh filter. Dried agglomerates were crushed to fine powder (up to 30 μm particle size). SEM image of the resulting powder shown in Fig. 1 proves successful formation of the layered silicates.

All materials were dried for 20 h prior to mixing to avoid bubble formation during filament extrusion. Mixing was carried out in a TSE20 Brabender twin-screw extruder with five heating zones (processing conditions are shown in Table 1). The resident time in the extruder was about 5 min. At the die exit, the extrudate was cooled on an elastic conveyor. In the next step, materials were converted to filaments of 3D-printer using a home-made single-screw extruder ($L/D = 20$, $D = 20$ mm) (Table 2) and finally, the dumb-bells and disks for tensile and rheological tests were printed using a 3D-printer of Sizan Company (Sizan^2 model). The printing process was carried out under the following conditions: Nozzle head and bed temperatures were set at 240 and 30 °C, respectively; nozzle moving

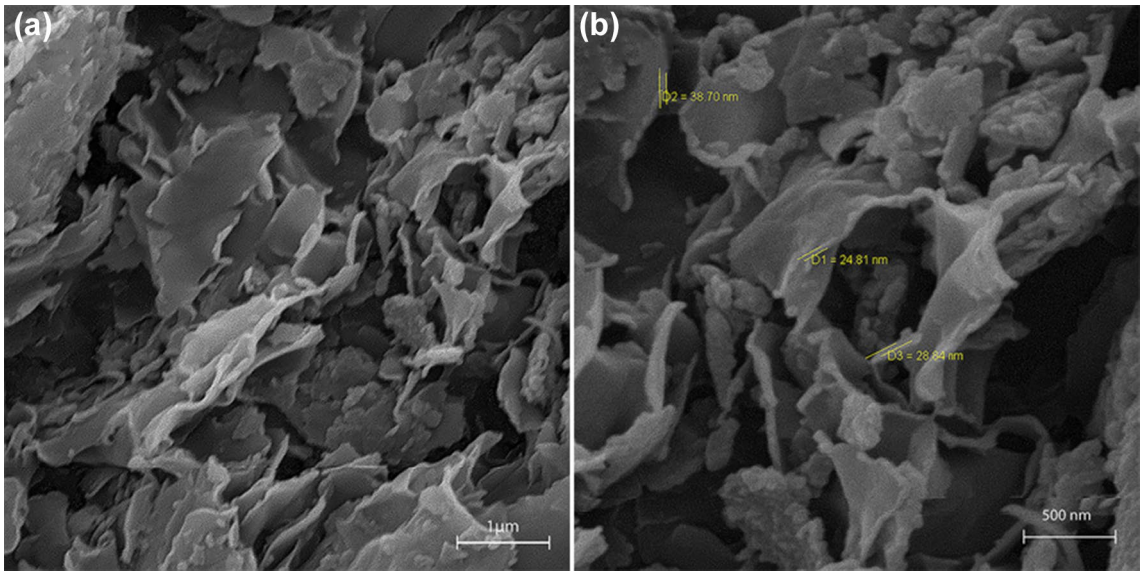

Fig. 1 SEM images of purified Mt

Table 1 The processing conditions in twin-screw extruder

Heating zone	1	2	3	4	5	Die
Temperature (°C)	195	200	200	200	210	220
Screw speed (rpm)	18.3					

Table 2 The processing conditions in single-screw extruder

Heating zone	1	2	Die
Temperature (°C)	190	200	220
Screw speed (rpm)	18.3		

Table 3 The composition of polypropylene composites

Sample	Bentonite	Cloisite 20A	PP	PP-*g*-MA
B1	0	0	80	20
B2	0	1.5	78.5	
B3	10	0	70	
B4	10	0.5	69.5	
B5	10	1	69	
B6	10	1.5	68.5	
B7	3	1	76	
B8	5	1	74	
B9	7	1	72	

speed for infilling was 100 mm/s, and the first layer thickness was set at 0.4 mm followed by 0.1 mm thickness for upper layers; and triangle infilling pattern with the starting angle of 45° was chosen. Formulations of nanocomposites are tabulated in Table 3.

The quality of dispersion and shape and morphology of the clusters were studied by a scanning electron microscope (SEM) (VEGA Tescan model, Czech Republic) equipped with energy-dispersive X-ray spectroscopy (EDX). The filaments were fractured in liquid nitrogen prior to metal coating and viewed by SEM.

Rheological measurement was carried out by MCR 501 rheometer by Anton Paar. Specimens were tested under a nitrogen atmosphere to prevent degradation of polymer chains as much as possible and we started from the lowest frequency possible with an instrument, from 0.01 to 600. In transient rheometry, the sample was rotationally strained at 0.3/s for 100 s. A composite disk was 10 min sheared and after a 10 min rest it was followed by further 10 min shearing to quantify the degree of polymer chain degradation.

Tensile tests were carried out on a Santam Universal Testing Machine (STM 20 model, Tehran, Iran) according to ASTM D638 at room temperature. Four dumb-bells were used for each test to ensure reproducibility (all printed using a Sizan^2 3D-printer). Mettler-Toledo apparatus was used for calorimetry at 10 °C/min heating rate under nitrogen atmosphere in the temperature range from − 50 to 240 °C

Table 4 Temperature and enthalpy crystallization and degree of crystallinity of samples

Sample	H_c (J/g)	X_c (%)	T_c (°C)
B1	100.58	47.78	116.25
B2	101.01	49.06	120.29
B5	92.06	49.78	123.51
B6	92.07	49.80	123.81

(Table 4). Small-angle X-ray scattering (SAXS) test was carried out using a Philips PW1730 (The Netherlands) employing a CuK_α as a radiation source with 1.5406 Å wavelength at 40 kV. The analysis was performed at 25 °C and d_{001} was calculated for the specimens using Bragg's equation ($n\lambda = 2d_{001}(\sin\theta)$).

Results and discussion

Clay dispersion in PP matrix

SEM micrographs were used to visualize clay layers distribution in the polymer matrix. Figure 2a, b corresponds to the surface fracture of sample B2. To unveil the dispersion quality of Cloisite 20A within the matrix, the composition of the surface fracture was measured by EDX as shown in Fig. 2c. It is clearly observed that the nanoclay particles have been well dispersed within the PP matrix. In addition, a smooth fracture surface is observable which can be attributed to uniform particle distribution and dispersion [19]. SEM image and corresponding EDX map of B3 sample are shown in Fig. 2d–f, accordingly. SEM studies

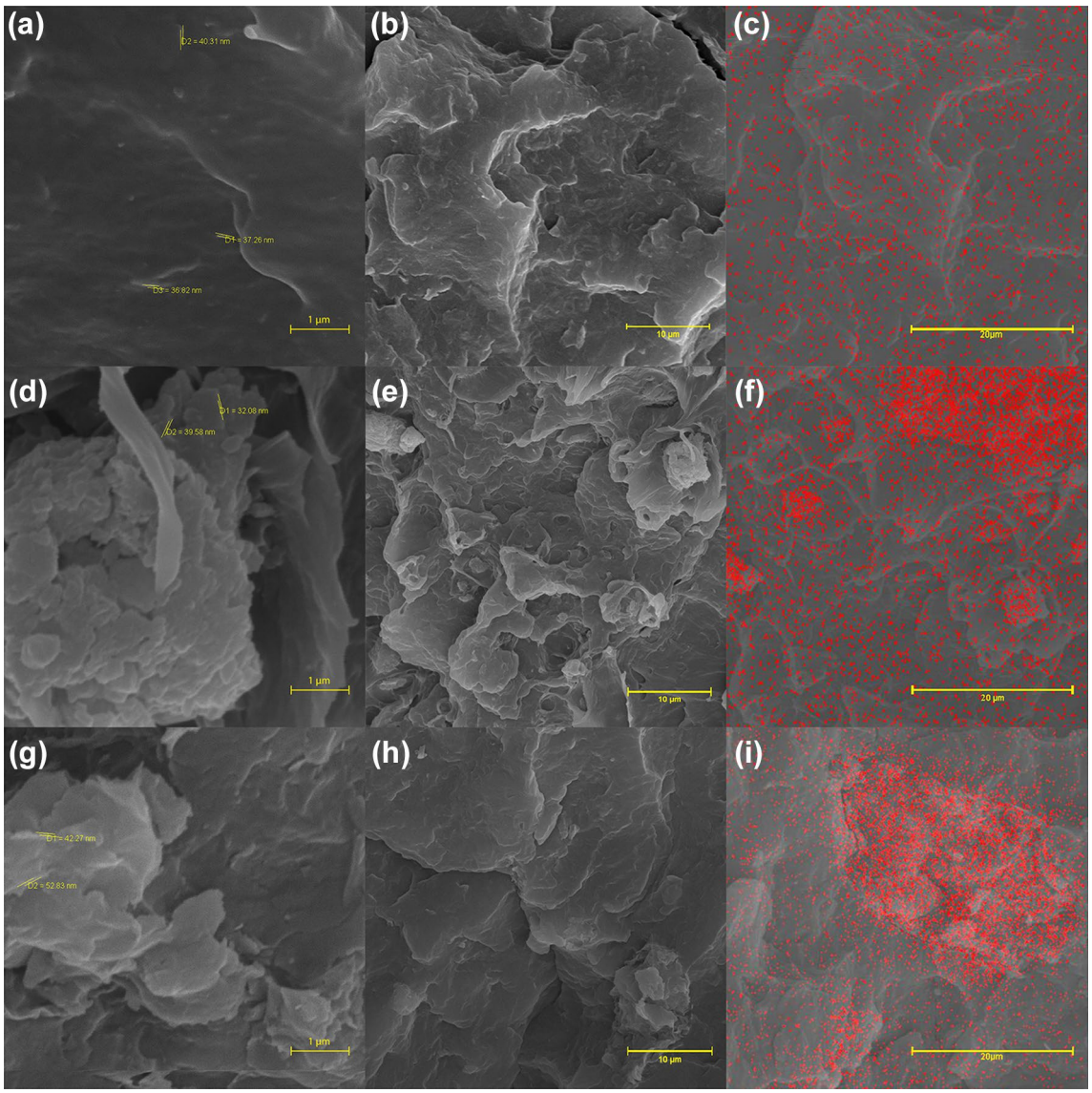

Fig. 2 **a** and **b** SEM images of B2, **c** EDX mapping of Si in B2, **d**, **e** SEM images of B3, **f** EDX mapping for Si in B3, **g**, **h** SEM images of B6 and **i** EDX mapping for Si in B6

clearly show a poor dispersion and distribution of purified Mt. Agglomeration of purified Mt could be related to low affinity of polymer chains towards purified Mt [20]. The size of agglomerates was measured to be about 7 µm. Figure 2g–i represents SEM images and EDX map of the hybrid composite containing Cloisite 20A and purified Mt nanosheets, accordingly. Microstructural study of B5 sample reveals that an increase in solid content does not lead to the formation of large agglomerates as observed in B3. The size of agglomerates was measured to be around 3 µm, twofolds smaller than those of B3. We believe that such an effect originates from sample processing conditions in molten state where due to their better interactions with polymer matrix organically modified nanoclay particles act as shear-transfer agents.

To further investigate the quality of dispersion of clay particles in PP matrix, small-angle X-ray scattering (SAXS) patterns of the original clay powders and with those of the composites were measured (Fig. 3). Neat Cloisite 20A powder shows a strong peak at 3.61°, whereas neat purified Mt does not show any peak in the studied 2θ range. Based on literature [19, 21] a peak at 8.87° is expected for natural Na^{+}Mt. According to Fig. 1, the Mt particles are very wide and thin which could be in a foam state (house-of-cards structure) [22–25] (Fig. 4). In this structure, the clay layers are far but inter-related with no peak at angles larger than 1°.

SAXS patterns could be used to study dispersion fineness in different composites (clay intercalation). The presence of a good dispersion in matrix of any kind of composite is a priority for attaining desired properties. In Fig. 3, SAXS patterns of different composites are reported, in which the main peak for B2 nanocomposite appeared at 3.24° which corresponds to $d_{001}=2.7$ nm (moderately exfoliated Cloisite 20A's *d*-spacing). The following curve implies that some layers have been exfoliated and others remained in existing clusters due to thermodynamic conditions and high surface energy [25, 26]. B3 microcomposite shows a peak at 8.87 with $d_{001}\sim1$ nm which

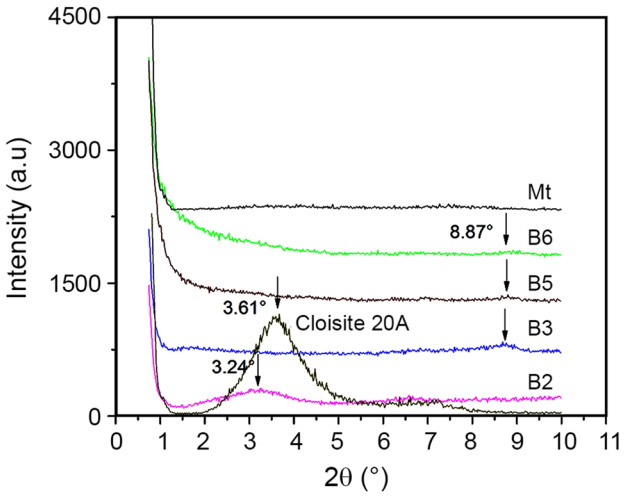

Fig. 4 X-ray diffraction patterns for micro, nano, and micro/nanocomposites

corresponds to inter-gallery distance of purified Mt which is repeated for all compositions of micro/nanocomposite. This is due to the fact that layers of Mt are not completely exfoliated at high solid contents in which some clusters re-agglomerate. Furthermore, B5 and B6 samples have weaker peaks at 8.87° and no peak at 3.24°. This indicates that clusters of Mt still exist in composite but all Cloisite 20A layers have been exfoliated [27]. This phenomenon occurs because of high surface energy of Mt and Cloisite along with lyophobic nature of silicate minerals. This leads to attraction of Cloisite particles by Mt and finally under high strains exerted by twin-screw extruder followed by high pressure developed at screw tip intercalation of Mt house-of-cards structure [28, 29]. Furthermore, a high solid content of micro/nanocomposite generates some extent of friction between the nanoclay and purified Mt which in turn leads to better intercalation of both clays in polymer matrix.

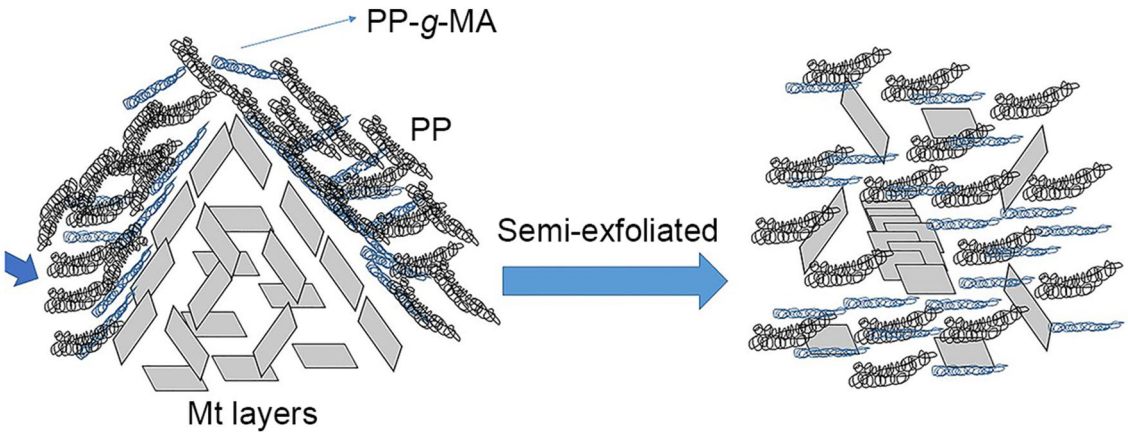

Fig. 3 Schematic illustration of house-of-card structure in the presence of shear

Nucleation and crystallization in nanocomposites

In Fig. 5, DSC thermograms were used to calculate crystal content and to estimate the nucleation effect at crystallization temperature. The crystallization content was calculated using the following equation:

$$X_c = 100 \times H_c / \Delta H_f^{\circ} \times w_{polymer},$$

where X_c is percent of crystallization, H_c the normalized enthalpy of nanocomposite, ΔH_f° (209 J/g) the fusion enthalpy of fully crystalline PP, and $w_{polymer}$ is the weight percentage of polymer in nanocomposite [30].

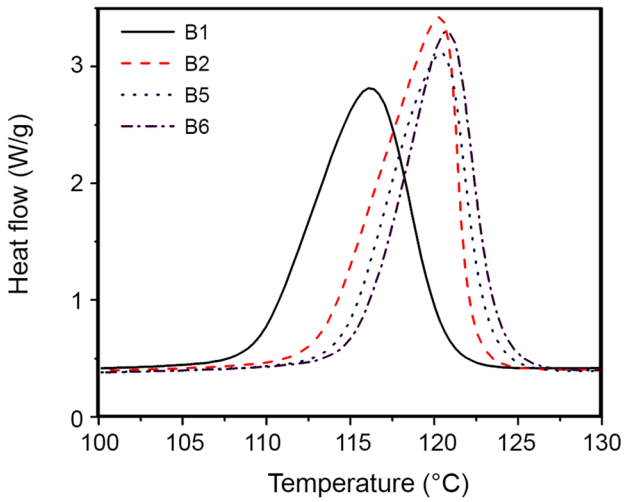

Fig. 5 DSC curves for micro, nano, and micro/nanocomposites

Upon incorporation of Cloisite 20A into neat polymer, both degree of crystallinity and crystallization temperature of polymer increased which indicates that nanoclay platens act as heterogeneous nuclei and restrain polymer chains to allow higher energy chains precipitate on a growing crystal lamella. Introducing Mt, new silicate layers come to act as new nuclei and consequently both degree of crystallinity and crystallization temperature in B5 sample. By increasing Cloisite 20A content in B6 sample, the degree of crystallinity remains almost intact but the temperature of crystallization increases slightly which shows that the mobility of chains is prohibited in the presence of Mt. Therefore, polymer crystals cannot grow anymore but changes in thermodynamics and the compatibilizer are still contributing toward crystallization because enthalpy quantities have been changed.

Rheological properties

Rheological measurements were also carried out on all samples in molten state. Rheological behavior of molten filament at nozzle of 3D-printer is very important and affects the final properties of all samples. Complex viscosity and storage modulus of samples are shown in Figs. 6 and 7. B1 sample showed the highest complex viscosity and storage modulus whereas addition of unmodified nanoclay sheets to PP in B3 sample decreases complex viscosity and storage modulus significantly. Both clay's weak interlayer interactions and extensive surface of nanoclay sheets prohibit polymer chains entanglements which may be responsible for these decreases. This behavior was also reported for polycarbonate/$CaCO_3$ system by Wang

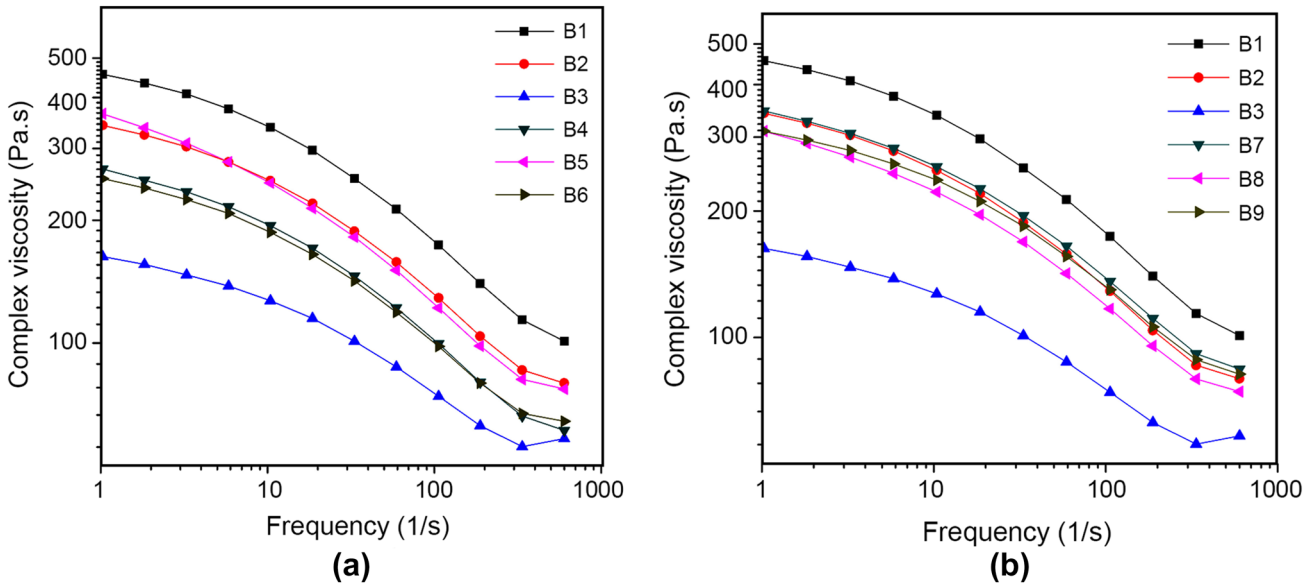

Fig. 6 Complex viscosity with frequency for different compositions: **a** Cloisite 20A and **b** Mt content were constant except of reference samples

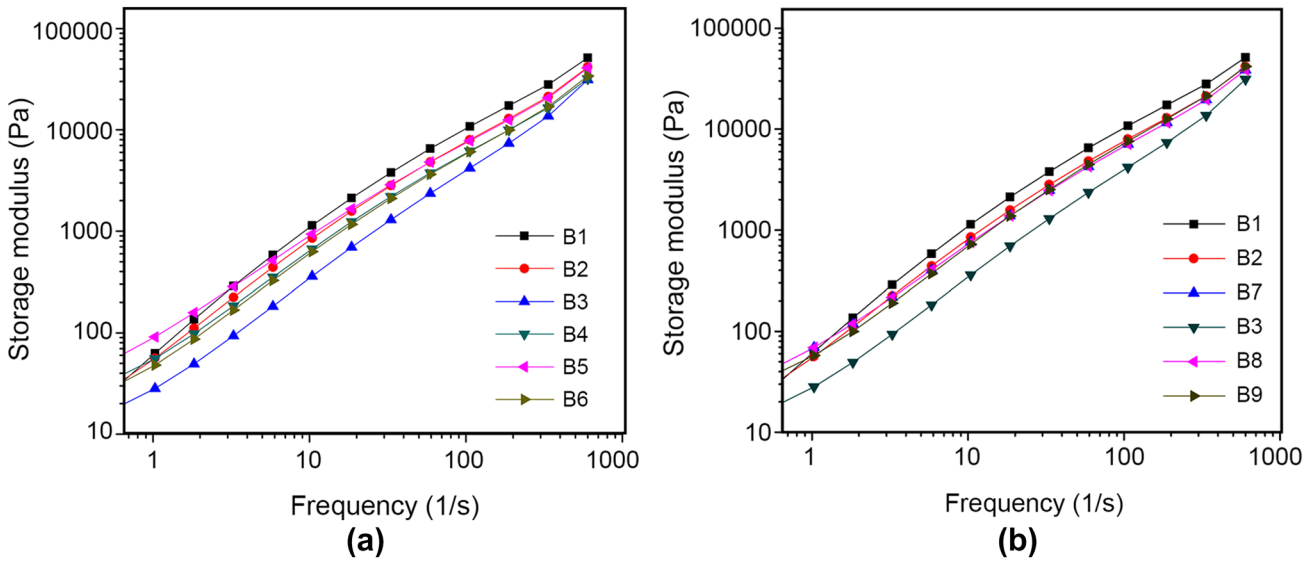

Fig. 7 Elastic modulus with frequency for different compositions: **a** Cloisite 20A and **b** Mt content were constant except of reference samples

et al. [31]. In Figs. 6 and 7, it is seen that the addition of organically modified nanoclay in B2 results in higher complex viscosity compared to that of B3. This could be attributed to higher interactions operated between modified layers of nanoclay and polymer matrix which lead to higher crystallization content and prevent sliding of the chains [32]. However, the extremely oriented layers of nanoclay are prohibiting entanglements, this extreme orientation is a result of 3D-printing technique which is very interesting [18]. The presence of modified and unmodified nanoclays in B4, B5, and B6 samples results in complex modulus variation (Fig. 6a). A meaningful synergy in B5 is observable with a higher complex viscosity compared to the average of those B2 and B3 samples. This is an optimum amount for modified nanoclay; adding more than that would increase agglomeration and less than that would decrease the reinforcing effect in B4 and B6. In Fig. 7a, the storage modulus is depicted for the same samples which confirmed our previous arguments. The interesting sample is B5 again which shows higher storage modulus at low frequencies that implies strong network of nanoclay created within the matrix.

In Fig. 6b, the content of unmodified nanoclay has been swept and the content of modified nanoclay has set to an optimum in the previous experiment. B7 sample shows a higher complex viscosity which indicates that adding more unmodified nanoclay would only intensify agglomeration and formation of clusters. As expected, B8 and B9 samples show lower complex viscosity and storage modulus (Figs. 6b, 7b).

Figure 8a is useful in explaining the extent of chain orientation in the samples. It shows that the 3D-printed sample shows a much lower complex viscosity compared to those of compression molded sample. This is an indication of exquisite degree of polymer chains-orientation that could be engineered in various ways. This could be considered as a criterion for the particle intercalation level in the nanocomposites which increases at higher degrees of exfoliation [8]. Also, a large overshoot has occurred for this particular composite that shows a strong network formation within the polymer matrix. A larger overshoot could only be attributed to formation of a stronger network under applied shear force [33]. The effect of the second shearing after the rest is shown in Fig. 8b. A reduction in the height of the overshoot in the second shearing could be assigned to polymer chain scission. As Fig. 8c reveals B2 sample has a small overshoot that suggests the formation of a network within polymer matrix. This overshoot surprisingly increases in the presence of purified Mt in B5 sample which is interpreted as synergetic effect resulting in higher intercalation of Mt layers [34, 35]. Furthermore, adding more Cloisite in B6 sample causes another massive increase in the observed overshoot, which cannot be produced by Cloisite's low contents. Compatibilization effect is another parameter which can explain the uphill slope of curve.

Mechanical analysis

In the following step, 3D-printed dumb-bells were subjected to tensile tests and the results are sketched in Figs. 9 and 10. The improvement in mechanical properties of nanocomposites as compared with those of conventional compression molding samples is evident [36]. Better mechanical properties are resulted by oriented polymer layers in case

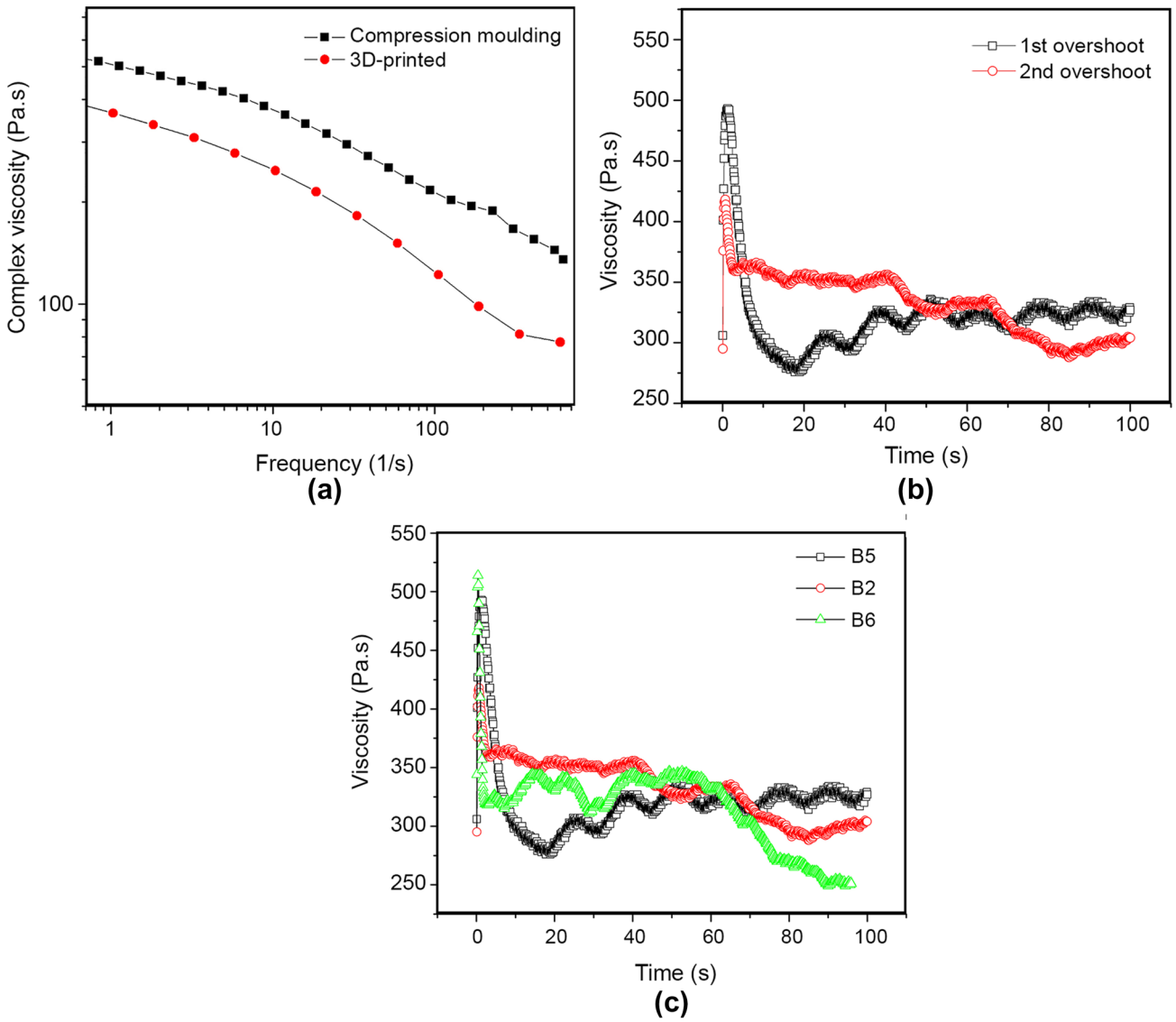

Fig. 8 **a** Comparison of complex viscosity of 3D-printed and compression molded B5 disks, **b** non-linear viscosity of B5 in degradation after some time for second rheometry, and **c** non-linear viscosity of B5, B2, and B6 nanocomposites

of printed dumb-bells which devote anisotropic properties to parts made for different applications. In Fig. 6, B1 represents the lowest modulus in which addition of Cloisite 20A and purified Mt leads to incremented Young's modulus. In solid state, the tensile properties were improved due to crystallization and chain entanglement during sample cooling, whereas in molten state complex viscosity and storage modulus decreased due to the absence of these two phenomena.

Increase in tensile modulus of these micro/nanocomposites resembles that of conventional composites because Mt does not take part in strong interactions with polymer chains. Therefore, a reinforcement effect is observed that is similar to that reported for additives [37]. In contrast, strain-at-break of B7 and B3 samples showed good extensions at break for B7 at low solid content. In case of B3, due to poor adhesion of Mt to polymer phase, no decrease in chain mobility is evident.

Figure 11 schematically represents the molten polymer filaments through the printer nozzle in extrusion process, where clay sheets are forced to orient in printing direction. Afterwards, polymer melt solidifies very fast due to the thinness of the polymer melt extruded through the nozzle and high surface area in contact with air. These arrangements cause polymer chains and clay layers become oriented in print direction. This orientation boosts mechanical properties and strain-at-break of the printed dumb-bells [38, 39].

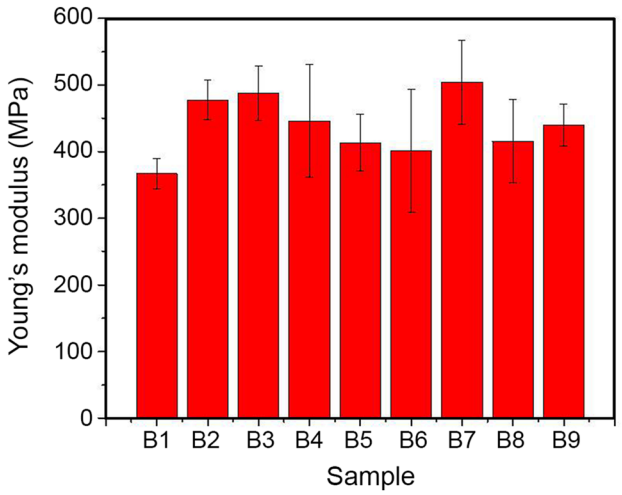

Fig. 9 Tensile modulus of nanocomposites

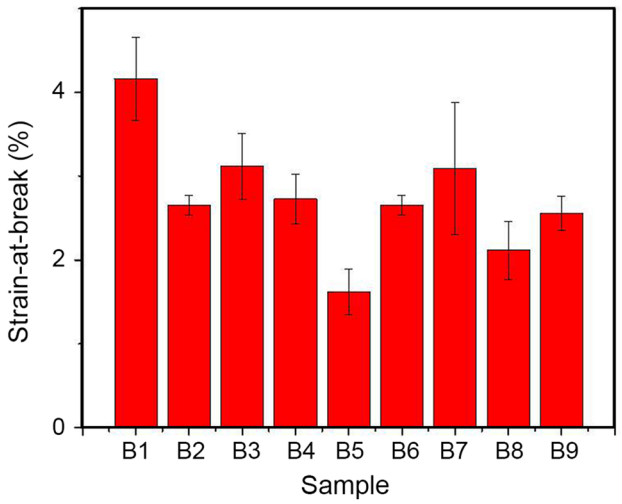

Fig. 10 Strain-at-break of nanocomposites

Conclusion

Use of PP-*g*-MA clearly affects shape and morphology of the clusters, and this new morphology contributes to intercalation of nanoclay layers which can be deduced from SEM and XRD. The new thermodynamics can be interpreted based on the increased rate of crystallization and its enthalpy. However, the most peculiar results are rheological values decrease due to highly oriented 3D-printed polymer chains and 60% increase in Young's modulus of some samples which is far above of what was measured for compression molded samples. PP-*g*-MA is a well-known compatibilizer for nanoclay's composites in different processing techniques. Despite this, no research has been reported on the use of this

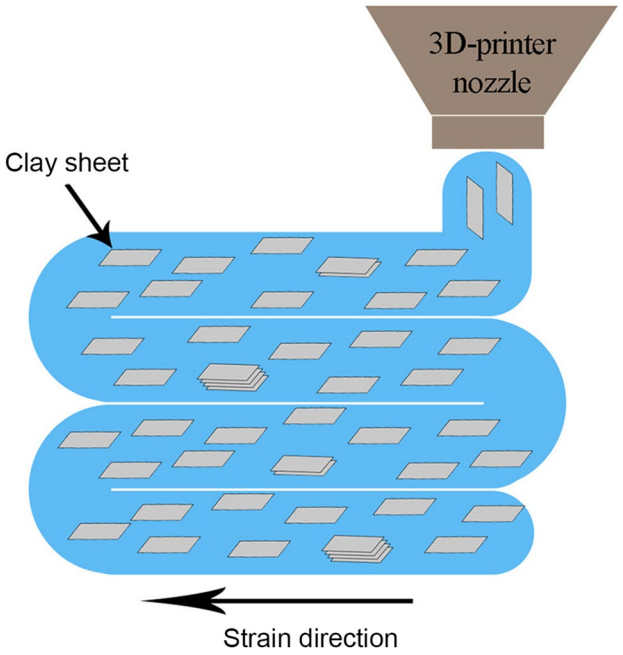

Fig. 11 Schematic image of 3D-printer nozzle and orientation in layers consequential by severe strain

material in 3D-printing filaments. With this fact in mind, the study on this material was conducted. SEM images and SAXS patterns proved intercalation along with some local agglomerations. Due to high contents of clay some clay sheets could not become intercalated or agglomerated again. Crystallization temperature of polymer phase increased and clay sheets, as heterogeneous nuclei, were found responsible for higher crystallinity. The most fascinating and peculiar behavior was observed in storage modulus and complex viscosity of composites which showed a decrease with addition of clay sheets. This phenomenon took place due to extensive orientation of polymer chains inside and through 3D-printer nozzle. High shears were employed in this zone-orient polymer chains alongside clay sheets and result in excessive shear thinning of this complex fluid. Finally, enhancement in mechanical properties of 3D-printed samples was about 60% (for some samples) which was much superior compared to those reported for compression molding samples.

References

1. Manias E, Touny A, Wu L, Strawhecker K, Lu B, Chung TC (2001) Polypropylene/montmorillonite nanocomposites. Review of the synthetic routes and materials properties. Chem Mater 13:3516–3523
2. Zhang S, Horrocks AR (2003) A review of flame retardant polypropylene fibres. Prog Polym Sci 28:1517–1538

3. Wong KV, Hernandez A (2012) A review of additive manufacturing. ISRN Mech Eng 2012:208760
4. Kojima Y, Usuki A, Kawasumi M, Okada A, Kurauchi T, Kamigaito OJ (1993) Synthesis of nylon 6-clay hybrid by MMT intercalated with ε-caprolactam. J Polym Sci Part A Polym Chem 31:983–986
5. Kojima Y, Usuki A, Kawasumi M, Okada A, Kurauchi T, Kamigaito O, Kaji K (1994) Fine structure of nylon-6/clay hybrid. J Polym Sci Part B Polym Phys 32:625–630
6. Zanetti M, Lomakin S, Camino G (2000) Polymer layered silicate nanocomposites. Macromol Mater Eng 279:1–9
7. Wang Y, Chen FB, Wu KC (2005) Effect of the molecular weight of maleated polypropylenes on the melt compounding of polypropylene/organoclay nanocomposites. J Appl Polym Sci 97:1667–1680
8. Wang Z, Xie G, Wang X, Li G, Zhang Z (2006) Rheology enhancement of polycarbonate/calcium carbonate nanocomposites prepared by melt-compounding. Matter Lett 60:1035–1038
9. Lertwimolnun W, Vergnes B (2005) Influence of compatibilizer and processing conditions on the dispersion of nanoclay in a polypropylene matrix. Polymer 46:3462–3471
10. Dubnikova IL, Berezina SM, Korolev YM, Kim GM, Lomakin SM (2007) Morphology, deformation behavior and thermomechanical properties of polypropylene/maleic anhydride grafted polypropylene/layered silicate nanocomposites. J Appl Polym Sci 105:3836–3850
11. García-López D, Gobernado-Mitre I, Merino JC, Pastor J (2007) Effect of the amount and functionalization grade of PP-*g*-MA compatibilization agent in polypropylene/clay nanocomposites. Polym Bull 59:667–676
12. Santos KS, Liberman SA, Oviedo MAS, Mauler RS (2014) Polyolefin-based nanocomposites: the effect of organosilane on organoclay dispersion. J Mater Sci 49:70–78
13. Chen H, Wang M, Lin Y, Chan CM, Wu J (2007) Morphology and mechanical property of binary and ternary polypropylene nanocomposites with nanoclay and $CaCO_3$ particles. J Appl Polym Sci 106:3409–3416
14. Sorrentino L, Berardini F, Capozzoli MR, Amitrano S, Iannace S (2009) Nano/micro ternary composites based on PP, nanoclay, and $CaCO_3$. J Appl Polym Sci 113:3360–3367
15. Zhang J, Han B, Zhou NL, Fang J, Wu J, Ma ZM, Shen J (2011) Preparation and characterization of nano/micro calcium carbonate particles/polypropylene composites. J Appl Polym Sci 119:3560–3565
16. Stoof D, Pickering K (2018) Sustainable composite fused deposition modelling filament using recycled pre-consumer polypropylene. Compos Part B Eng 135:110–118
17. Haigh JN, Dargaville TR, Dalton PD (2017) Additive manufacturing with polypropylene microfibers. Mater Sci Eng C 77:883–887
18. Sodeifian GR, Gahseminezhad S, Yousefi AA (2019) Preparation of polypropylene/short glass fiber composite as fused deposition modeling (FDM) filament. Result Phys 12:205–222
19. Morreale M, Dintcheva NT, La Mantia FP (2011) The role of filler type in the photo-oxidation behaviour of micro and nano filled polypropylene. Polym Int 60:1107–1116
20. Sharma SK, Nayak SK (2009) Surface modified clay/polypropylene (PP) nanocomposites: effect on physico-mechanical, thermal and morphological properties. Polym Degrad Stab 94:132–138
21. Hasegawa N, Okamoto H, Kato M, Usuki A, Sato N (2003) Nylon 6/Na–montmorillonite nanocomposites prepared by compounding nylon 6 with Na–montmorillonite slurry. Polymer 44:2933–2937
22. Laske S (2015) Polymer nanoclay composites, Chap. 1. Elsevier (Imprint:Wiliam Andrew), Amsterdam, pp 10–11
23. Okamoto M (2003) Polymer/layered silicate nanocomposites, vol 14. Ismithers Rapra Publishing, Shropshire, pp 48–53
24. Haraguchi K, Li HJ (2006) Mechanical properties and structure of polymer–clay nanocomposite gels with high clay content. Macromolecules 39:1898–1905
25. Alekseeva OV, Rodionova AN, Bagrovskaya NA, Noskov AV, Agafonov AV (2019) Bentonite filler effect on structure and properties of polystyrene-based composites. Iran Polym J 28:123–133
26. Zare Y, Garmabi H (2012) Analysis of tensile modulus of PP/nanoclay/$CaCO_3$ ternary nanocomposite using composite theories. J Appl Polym Sci 123:2309–2319
27. Chrissopoulou K, Anastasiadis SH (2011) Polyolefin/layered silicate nanocomposites with functional compatibilizers. Eur Polym J 47:600–613
28. Osswald T, Hernández-Ortiz JP (2006) Polymer processing. Hanser, Munich, pp 126–132
29. Rauwendaal C (2014) Polymer extrusion, 4th edn. Hanser, Munich, pp 576–590
30. Patnaik KR, Devi KS, Kumar VK (2010) Non-isothermal crystallization kinetics of polypropylene (PP) and polypropylene (PP)/talc nanocomposite. Int J Chem Eng Appl 1:346–355
31. Wang K, Liang S, Deng J, Yang H, Zhang Q, Fu Q, Dong X, Wang D, Han CC (2006) The role of clay network on macromolecular chain mobility and relaxation in isotactic polypropylene/organoclay nanocomposites. Polymer 47:7131–7144
32. Zadhoush A, Reyhani R, Naeimirad M (2019) Evaluation of surface modification impact on PP/MWCNT nanocomposites by rheological and mechanical characterization, assisted with morphological image processing. Polym Compos 40:E501–E510
33. Nazockdast E, Nazockdast H, Goharpey F (2008) Linear and nonlinear melt state viscoelastic properties of polypropylene/organoclay nanocomposites. Polym Eng Sci 48:1240–1249
34. Li J, Zhou C, Wang G, Zhao D (2003) Study on rheological behavior of polypropylene/clay nanocomposites. J Appl Polym Sci 89:3609–3617
35. Solomon MJ, Almusallam AS, Seefeldt KF, Somwangthanaroj A, Varadan P (2001) Rheology of polypropylene/clay hybrid materials. Macromolecules 34:1864–1872
36. Carneiro OS, Silva AF, Gomes R (2015) Fused deposition modeling with polypropylene. Mater Des 83:768–776
37. Shahmirzadi SR, Yousefi AA, Naderpour N (2016) Morphology and rheological properties of copper–polypropylene composite as a candidate for fusion deposition modeling (FDM) filament. In: ISPST 2016, Islamic Azad University, Tehran
38. Morits M, Verho T, Sorvari J, Liljeström V, Kostiainen MA, Gröschel AH, Ikkala O (2017) Toughness and fracture properties in nacre-mimetic clay/polymer nanocomposites. Adv Funct Mater 27:1605378
39. Suter JL, Groen D, Coveney PV (2015) Chemically specific multiscale modeling of clay–polymer nanocomposites reveals intercalation dynamics, tactoid self-assembly and emergent materials properties. Adv Mater 27:966–984